Brain Structure and Function (2019) 224:2269–2280
https://doi.org/10.1007/s00429-019-01883-z

SHORT COMMUNICATION

Transcriptomic profile of the subiculum-projecting VIP GABAergic neurons in the mouse CA1 hippocampus

Xiao Luo[1,2] · Einer Muñoz-Pino[1,2] · Ruggiero Francavilla[1,2] · Maxime Vallée[3,4] · Arnaud Droit[3] · Lisa Topolnik[1,2]

Received: 16 March 2018 / Accepted: 2 May 2019 / Published online: 16 May 2019

Abstract

In cortical circuits, the vasoactive intestinal peptide (VIP+)-expressing GABAergic cells represent a heterogeneous but unique group of interneurons that is mainly specialized in network disinhibition. While the physiological properties and connectivity patterns have been elucidated in several types of VIP+ interneurons, little is known about the cell type-specific molecular repertoires important for selective targeting of VIP+ cell types and understanding their functions. Using patch-sequencing approach, we analyzed the transcriptomic profile of anatomically identified subiculum-projecting VIP+ GABAergic neurons that reside in the mouse hippocampal CA1 area, express muscarinic receptor 2 and coordinate the hippocampo-subicular interactions via selective innervation of interneurons in the CA1 area and of interneurons and pyramidal cells in subiculum. We explored the VIP+ cell gene expression within major gene families including ion channels, neurotransmitter receptors, neuromodulators, cell adhesion and myelination molecules. Among others, a large variety of genes involved in neuromodulatory signaling, including acetylcholine (*Chrna4*), norepinephrin (*Adrb1*), dopamine (*Drd1*), serotonin (*Htr1d*), cannabinoid (*Cnr1*), opioid (*Oprd1, Oprl1*) and neuropeptide Y (*Npy1r*) receptors was detected in these cells. Many genes that were enriched in other local VIP+ cell types, including the interneuron-selective interneurons and the cholecystokinin-coexpressing basket cells, were detected in VIP+ subiculum-projecting cells. In addition, the neuronatin (*Nnat)* and the Purkinje Cell Protein 4 (*Pcp4*) genes, which were detected previously in long-range projecting GABAergic neurons, were also common for the subiculum-projecting VIP+ cells. The expression of some genes was validated at the protein level, with proenkephalin being identified as an additional molecular marker of this VIP+ cell type. Together, our data indicate that the VIP+ subiculum-projecting cells share molecular identity with other VIP+ and long-range projecting GABAergic neurons, which can be important for specific function of these cells associated with their local and distant projection patterns.

Keywords Inhibition · Subiculum-projecting GABAergic cell · Vasoactive intestinal peptide · Patch-sequencing

Introduction

Understanding brain computations requires a detailed analysis of single neurons, from gene expression to cell-specific network and behaviour function. GABAergic inhibitory interneurons constitute one of the most heterogeneous neuronal populations in cortical networks, as dozens of different interneuron types with specific morphological and physiological properties have been described so far (Petilla Interneuron Nomenclature et al. 2008; Somogyi, 2010). While some interneuron types (e.g., parvalbumin-expressing basket or somatostatin-positive Martinotti cells) have been well characterized at a structural and functional level, the other rare types remain unstudied. This is particularly the case for the vasoactive intestinal peptide-expressing (VIP+) interneurons that derive from the

Electronic supplementary material The online version of this article (https://doi.org/10.1007/s00429-019-01883-z) contains supplementary material, which is available to authorized users.

✉ Lisa Topolnik
Lisa.topolnik@bcm.ulaval.ca

[1] Department of Biochemistry, Microbiology and Bio-informatics, Université Laval, Québec, PQ G1V 0A6, Canada

[2] Neuroscience Axis, CHU de Québec Research Center, Université Laval, Québec, PQ G1V 4G2, Canada

[3] CHU de Québec Research Center, Université Laval, Québec, Canada

[4] Department of Molecular Medicine, Laval University, Québec, PQ G1V 4G2, Canada

caudal ganglionic eminence (CGE) (Miyoshi et al. 2015) and account for ~ 10–15% of GABAergic interneurons in the neocortex (Gonchar et al. 2007). Recent findings highlighted the critical role of VIP+ interneurons in regulating complex behavioural tasks, such as reward-associated learning, visual processing and locomotion through local network disinhibition (Lee et al. 2013; Pi et al. 2013; Fu et al. 2014; Ayzenshtat et al. 2016). However, these cells are also heterogeneous and can exhibit distinct morphological and neurochemical properties as well as cell-specific connectivity patterns and physiological roles (Acsády et al. 1996a, b; Porter et al. 1998; Bayraktar et al. 2000; Chamberland et al. 2010; Tyan et al. 2014). In addition to VIP+ interneuron-selective cells targeting local interneurons (Acsády et al. 1996a, b; Chamberland et al. 2010; Tyan et al. 2014) and VIP+ basket cells (Somogyi et al. 2004), a novel type of VIP/muscarinic receptor 2 (M2R)-co-expressing subiculum-projecting GABAergic neuron has been identified in the CA1 hippocampus (Francavilla et al. 2018). These cells target interneurons in the CA1 and both interneurons and principal cells in subiculum. Unlike other GABAergic cells in the hippocampus (Klausberger and Somogyi 2008), subiculum-projecting VIP+ cells are more active during quiet wakefulness and are not involved in theta and ripple oscillations. However, the molecular profile of these cells, which would help to target them for selective manipulations and functional studies remains unknown.

Recent advances in opto- and pharmacogenetic technologies and the development of cell-specific transgenic targeting strategies allowed the manipulation of specific cellular populations. For example, a large set of mouse lines based on the Cre/Flp and Cre/Dre double recombinase systems has been generated for highly selective manipulations (Taniguchi et al. 2011; Madisen et al. 2015; He et al. 2016; Paul et al. 2017). However, the ongoing development of cell-specific mouse lines requires identification of cell-specific markers. Next generation single-cell RNA sequencing (scRNA-seq) has proved to be a powerful tool in neuronal transcriptomic profiling (Zeisel et al. 2015; Tasic et al. 2016; Paul et al. 2017). Importantly, when combined with patch-clamp recordings (Patch-seq), it allows the acquisition of single-cell transcriptomes from morphologically and electrophysiologically identified neurons, thus providing a unique opportunity for multimodal sampling of rare cell types (Cadwell et al. 2016; Fuzik et al. 2016; Foldy et al. 2016). Here, we used this approach to explore the transcriptomic profile of the hippocampal CA1 subiculum-projecting cells, a sparse GABAergic population, which is positioned to control the information flow along the hippocampo-subicular axis and to coordinate the two functionally related areas. We provide single-cell transcriptomes of the subiculum-projecting VIP+ cells and identify some molecular markers that can be used for their combinatorial targeting.

Materials and methods

Experimental subjects and housing conditions

We used the previously characterized VIP/enhanced green fluorescent protein (VIP-eGFP; Tyan et al. 2014) mice [BAC line with multiple gene copies; MMRRC strain #31009, STOCK Tg (Vip-EGFP) 37Gsat, University of California, Davis, CA, USA]. Mice had access to food and water ad libitum and were housed in groups of two to four. All experiments were approved by the Animal Protection Committee of Université Laval and the Canadian Council on Animal Care.

Patch RNA-sequencing in acute hippocampal slices

Transverse hippocampal slices (thickness, 300 µm) were prepared from VIP-eGFP mice (P15–P25) of either sex as described previously (Tyan et al. 2014). Briefly, animals were anaesthetized deeply with isoflurane and decapitated. The brain was dissected and transferred into an ice-cold (0–4 °C) solution containing the following (in mM): 250 sucrose, 2 KCl, 1.25 NaH_2PO_4, 26 $NaHCO_3$, 7 $MgSO_4$, 0.5 $CaCl_2$, and 10 glucose oxygenated continuously with 95% O_2 and 5% CO_2, pH 7.4, 330–340 mOsm/L. Slices were cut using a vibratome (VT1000S; Leica Microsystems or Microm; Fisher Scientific), transferred to a heated (37.5 °C) oxygenated recovery solution containing the following (in mM): 124 NaCl, 2.5 KCl, 1.25 NaH_2PO_4, 26 $NaHCO_3$, 3 $MgSO_4$, 1 $CaCl_2$, and 10 glucose; pH 7.4; 300 mOsm/L and allowed to recover for 1 h. Subsequently, they were kept at room temperature until use. During experiments, slices were continuously perfused (speed: 2 mL/min; temperature: 30–33 °C) with standard artificial cerebrospinal fluid (ACSF) containing the following (in mM): 124 NaCl, 2.5 KCl, 1.25 NaH_2PO_4, 26 $NaHCO_3$, 2 $MgSO_4$, 2$CaCl_2$, and 10 glucose, pH 7.4 saturated with 95% O_2 and 5% CO_2. VIP-positive O/A interneurons were visually identified as eGFP-expressing cells upon illumination with blue light (filter set: 450–490 nm).

Glass capillaries and small tools were autoclaved before the experiment. All working surfaces were cleaned with DNA-OFF (Takara, Cat. No. 9036) and RNase Zap (Life Technologies, Cat. No. AM9780). The patch-clamp protocol was optimized to perform high-quality RNAseq of single morphologically identified neurons (Fuzik et al. 2016; Cadwell et al. 2016). In particular, to provide for optimal RNA yield, we kept the same pipette tip size, volume of patch-solution and a modified intracellular solution as in Cadwell et al. (2016). Patch pipettes with low resistance (2–4 MΩ) were filled with ~ 1 µl of intracellular solution

containing (in mM): 130 $KMeSO_4$, 2 $MgCl_2$, 10 diNa-phosphocreatine, 10 HEPES, 4 ATP-Tris, 0.4 GTP-Tris, glycogen (an inert carrier to increase the RNA recovery, 20 µg/ml; ThermoFisher Scientific), and 1.3 mg/ml biocytin, pH 7.2–7.4, 275–290 mOsm/L. Before approaching the cell of interest, 0.1–0.2 ml positive pressure was applied to the patch-pipette, and the pipette was quickly advanced through the slice until it was touching the cell membrane. Membrane properties were recorded in current-clamp mode within the first 5 min by subjecting cells to multiple current step injections of varying amplitudes (− 400 to + 280 pA). Data acquisition (filtered at 2–3 kHz and digitized at 10 kHz; Digidata 1440, Molecular Devices, CA, USA) was performed using the Multiclamp 700B amplifier and the Clampex 10.5 software (Molecular Devices). The whole-cell configuration was kept for 15–20 min to allow the diffusion of biocytin. The cell quality was evaluated according to electrophysiological (stable membrane potential of more than − 50 mV, and AP amplitude ≥ 50 mV measured from the threshold) criteria. Only cells of good quality were processed for complementary DNA (cDNA) library construction. RNA was collected at the end of the recording by slowly applying light suction of 0.2–0.3 ml through a syringe connected to the patch-pipette until the cell was shrunk or the gigaseal was lost. Both the cytoplasm and the nucleus were sampled, resulting in a high cDNA yield (Fig. 1d). Then the tip of the pipette was broken and the cell content was ejected into an RNase-free PCR tube containing 10 µl 1X lysis buffer and 1 µl RNase inhibitor, spun down to the bottom and stored at − 80 °C. If any tissue debris were observed on the pipette tip when withdrawn from the slice, the sample was discarded. The slices were fixed with 4% PFA and processed for biocytin labeling to recover the cell morphology. In negative control (Ctl "–") experiments, the samples were obtained by aspirating tissue in O/A using the same approach and suction procedures. Positive control (Ctl "+") was obtained by sequential aspiration of 3 GFP+ O/A cells into the same patch-pipette (Fig. 1f).

The cDNA libraries were constructed using SMART-Seq v4 Ultra low input RNA Kit (Clontech Laboratories, Takara Bio; Mountain View, CA, USA). The first-strand cDNA was synthesized from cell contents by the 3′ SMART-Seq CDS Primer II A and template switching was performed by SMART-Seq v4 Oligonucleotide at the 5′ end of the transcript. Then cDNA from SMART sequences was amplified by PCR Primer II A. After 17 cycles of long-distance PCR, amplified cDNA was purified using the Agencourt AMPure XP Kit (Beckman Coulter, Cat. No. A63882). The quality of cDNA library construction was validated using the Agilent Tapestation 2200 system. The threshold cDNA concentration of 200 pg/ml (Cadwell et al. 2016) was achieved in all samples. Subsequently, cDNA libraries were prepared for Illumina Next-Generation Sequencing using Nextera XT DNA Library Preparation Kits (Illumina Inc., San Diego, CA, USA). Libraries with unique index were then pooled together in equimolar ratio and sequenced for paired-end sequencing using both lanes of a rapid run flow-cell on the Illumina HiSeq 2500 system. The average insert size for the paired-end libraries was 225 base pairs. Investigators conducting the cDNA library construction were blind to the experimental condition (cell *vs* Ctl"–" vs Ctl"+").

Analysis of patch RNAseq data

Given that the External RNA Controls Consortium (ERCC) spike-in-based approach may not be appropriate for quantifying technical noise, quality control assessment and absolute transcript normalization (Brennecke et al. 2013; Grun and van Oudenaarden 2015; Risso et al. 2014), this method was not used in our analysis of single-cell samples. Sequencing raw data were de-multiplexed to discriminate reads from different samples and then trimmed to remove sequencing adapters, low confidence bases, sequencing-specific bias and PCR artifacts. We computed reads alignments as a measure of quality, specifically the fraction of reads that could be mapped back to the mouse genome (mm10 assembly) as indicated by the aligner STAR (v2.5.2a). For reads quantification we computed pseudo-alignments using Kallisto (Pachter Lab, UC Berkeley). The average number of pseudo-aligned reads per cell was 2.1 million. Expression levels in individual cells were presented in TPM (transcripts per million; with TPM threshold set to 1.0 to filter out noise from the expression data). The number of genes with TPM values ≥ 1.0 varied from 4000 to 16,000 (Fig. 1e) and was in the range of the previously reported with Patch-seq (e.g., 7,000 genes/cell in Cadwell et al. (2016); 4000–10,000 genes/cell in Fuzik et al. 2016), thus validating our protocol. Out of 32 cells processed in these experiments, only 7 cells could be identified post hoc as projecting to subiculum (Fig. 1b) and showing no contamination by glial and excitatory neuronal transcripts (Fig. 1f). We also confirmed the phenotype of the subiculum-projecting VIP+ cells by verifying the M2R + expression in their dendrites (Fig. 1c). These cells were included in subsequent gene expression analysis (Fig. 2, 3 and 4). The gene expression data are presented in TPM values using a base-2 log scale. Investigators were blind to the condition (sample *vs* control) during analysis. Statistical analysis for the expression levels of common genes and selected genes was performed using one-way ANOVA test (Fig. 2b–d).

Accession numbers: The RNA-sequencing raw data associated with this manuscript have been uploaded to GEO (accession # GSE109755).

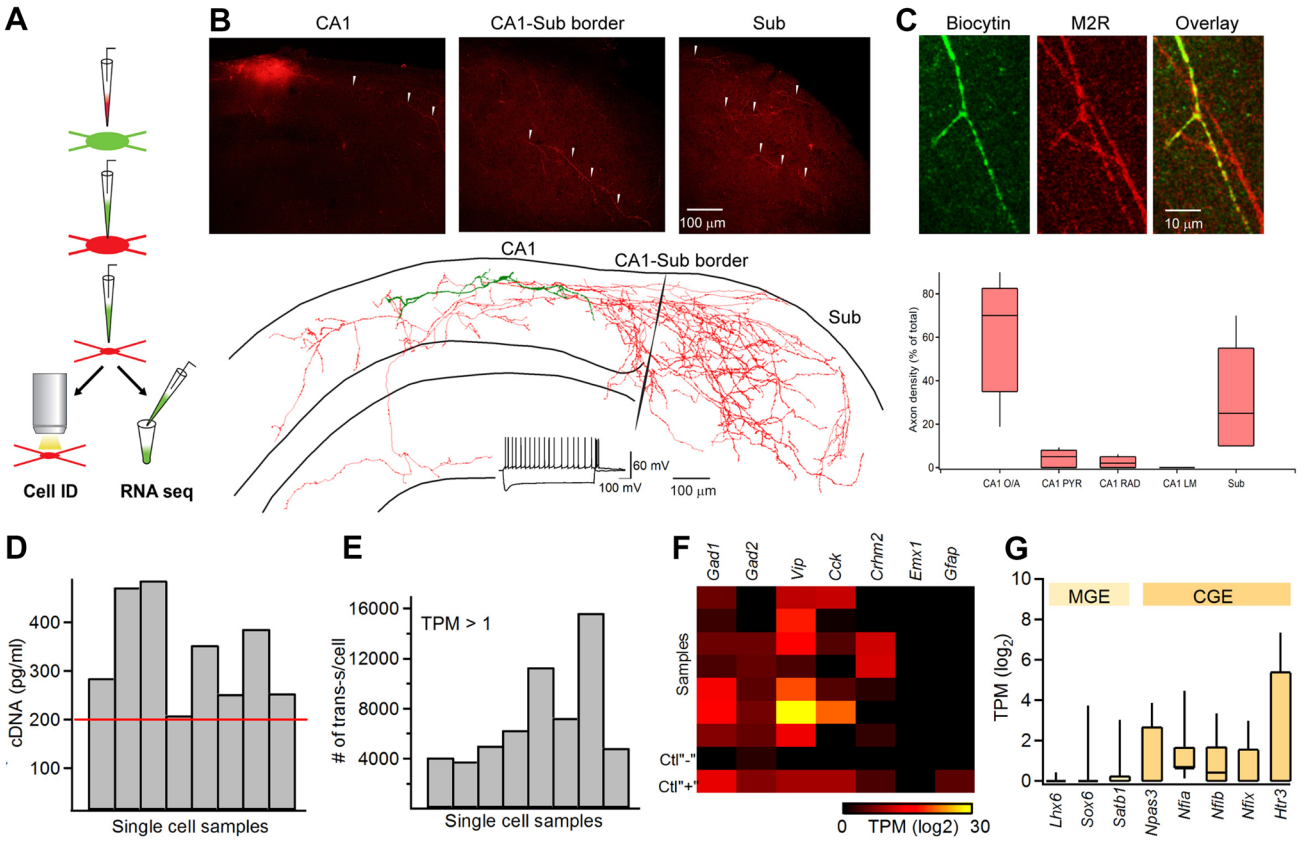

Fig. 1 Patch-sequencing of the subiculum-projecting VIP+cells. **a** Schematic of patch RNAseq experiment. **b** Examples of confocal images (single focal plans) showing the morphology of cell (top; arrowheads point to the axon leaving the CA1 O/A and making branches in the subiculum) and a corresponding Neurolucida reconstruction along with a typical membrane potential responses to current injections (bottom). Dendrites and soma are shown in green, axon in red; current steps of – 400 pA and + 60 pA were applied to evoke membrane potential responses. **c** Immunolabelling for M2R in dendrites of a VIP subiculum-projecting cell filled with biocytin and used for patch-seq analysis (top), and the summary box plot showing the axonal density in different CA1 layers and in subiculum obtained from nine reconstructed neurons (bottom). **d** Bar graph showing the concentration of cDNA (with red line indicating the 200 pg/ml threshold used as a criterion for sample inclusion as in Cadwell et al. 2016). **e** Bar graph showing the number of transcripts per sample (with TPM > 1) generated in single cell sequencing experiments. **f** Heat-map showing the expression of some VIP interneuron genes (*Gad1, Gad2*; *Vip, Cck, Chrm2*) and the absence of excitatory (*Emx1*) and glial (*Gfap*) transcripts in single-cell samples selected for further analysis ($n = 7$ cells; based on post hoc identification of axonal projections and quality control criteria). Negative control (Ctl"–") line illustrates the expression of the same transcripts in sample obtained by aspiration of extracellular matrix. Positive control (Ctl"+") line shows the expression of genes following the sequential aspiration of three GFP+ interneurons (without post hoc anatomical analysis) in the same patch-pipette for combined analysis. **g** Summary boxplots of some MGE- and CGE-specific genes show preferential expression of CGE-genes in VIP subiculum-projecting cells

Cell reconstruction and immunohistochemistry

For post hoc reconstruction, neurons were filled with biocytin (Sigma) during whole-cell recordings. Slices with recorded cells were fixed overnight with 4% paraformaldehyde (PFA) at 4 °C. To reveal biocytin, the slices were permeabilized with 0.3% Triton X-100 and incubated at 4 °C with streptavidin-conjugated Alexa-488 or Alexa-546 (1:1000) in TBS.

For patch-seq validation, immunohistochemical tests were performed on free-floating sections (40 µm thick) obtained with Leica VT1000S vibratome from 3 to 4 mice (20 sections/animal) per condition. VIP-eGFP mice were perfused with 4% PFA and the brains were sectioned. Sections were permeabilized with 0.25% Triton X-100 in PBS containing normal donkey serum (10%) and incubated overnight at 4 °C with primary antibodies (1:1000, chicken anti-eGFP, GFP-1020, Aves; 1:2000, rat anti-M2R, MAB367, Millipore; 1:500, goat anti-mGluR1a, mGluR1a-Go-Af1220, Frontier Institute; 1:250, rabbit anti-NPY, 22940, Immunostar; 1:500, rabbit anti-Netrin G1, GTX115637, Genetex; 1:500, rabbit anti-proenkephalin, LS-C23084, Lifespan Biosciences) followed by the incubation with secondary antibodies (donkey anti-chicken Alexa-488; donkey anti-rat

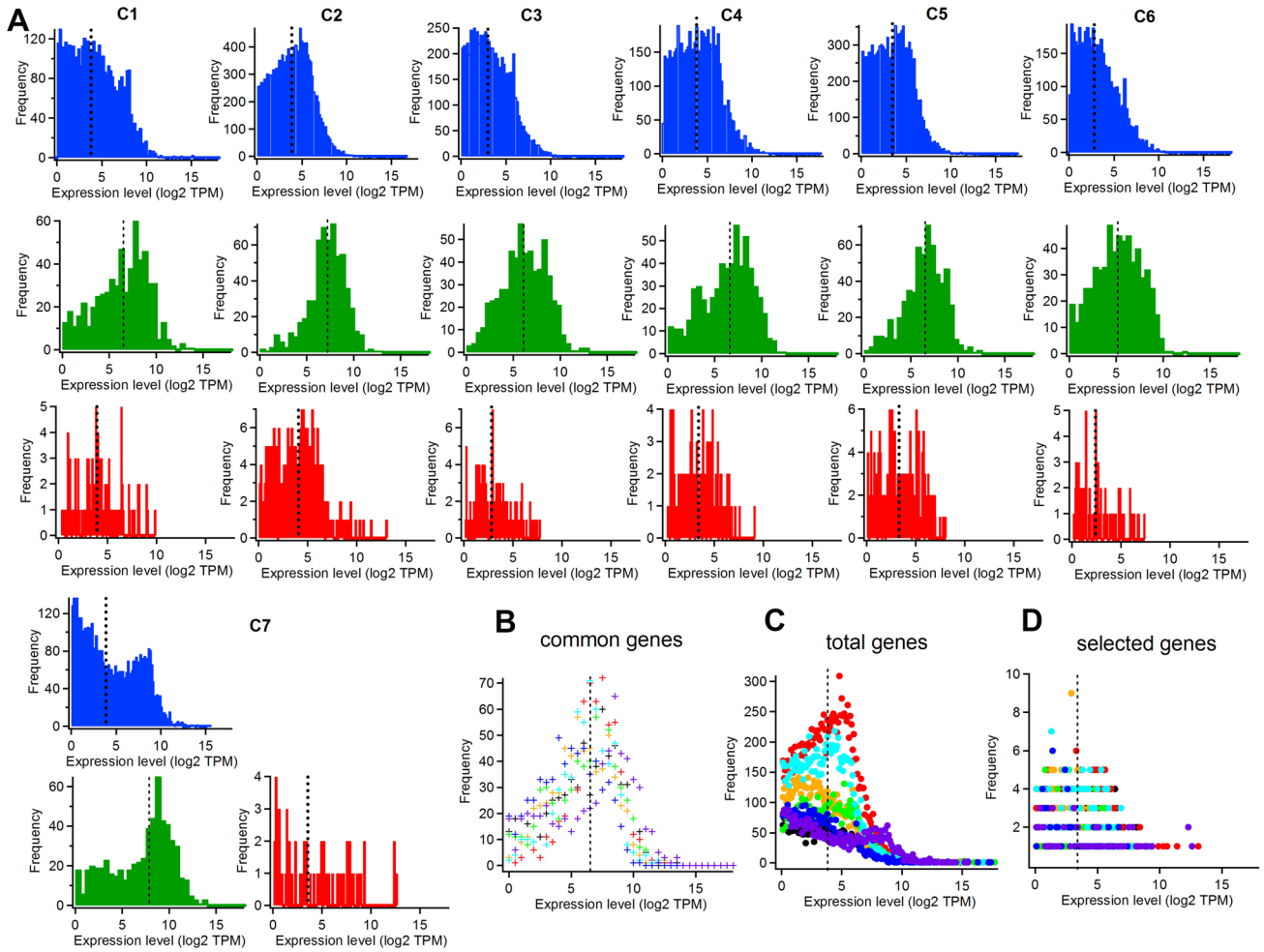

Fig. 2 Frequency distribution of total genes, common genes and genes selected based on functional families for each single cell sample. **a** Histograms of gene frequencies (blue: total genes; green: common genes expressed in all 7 samples and shown in Table 1; red: genes selected based on functional families and shown in Supplementary Table 2) at different expression levels for each single cell (c1–c7). Horizontal axis: expression level shown in log2 TPM. Vertical axis: gene frequencies that fall into each bin of the expression level. The bin size was determined automatically in Igor Pro 4.0. The frequency distribution of total genes, selected genes, and common genes follow the same trends from low to high expression values. The medians of gene expression levels are depicted as dashed lines and were similar between total genes and selected genes within the same cell. The common genes (green) showed a significantly higher expression level in all samples ($P < 0.001$ for all cells, one-way ANOVA). **b–d** Superimposed frequency distribution of common genes (**b**) total genes (**c**) and selected genes (**d**). Different colors represent different single cell samples. Each dot represents the number of genes within a 0.1 $\log_2$ TPM bin

CF-633; donkey anti-goat Cy3; donkey anti-rabbit Alexa-546). For proenkephalin and Netrin G1 immunoreactions, biotinylation was performed to enhance the labeling specificity. Briefly, following overnight incubation of sections with rabbit proenkephalin or Netrin G1 primary antibodies, biotinylated anti-rabbit antibody was applied for 24 h followed by streptavidin-conjugated AlexaFluor-546 (1:1000). For controlling method specificity, the primary antibodies were omitted and sections incubated in the full mixture of secondary antibodies. Under such conditions, no selective cell labeling was detected. Confocal images were acquired sequentially using a Leica TCS SP5 imaging system coupled with a 488-nm argon, a 543-nm HeNe and a 633-nm HeNe lasers. *Z* stacks of biocytin-filled cells were acquired with a 1-µm step and merged for reconstruction in Neurolucida 8.26.2.

Results

This study focused on a population of the M2R-expressing VIP+ GABAergic neurons that reside in the oriens/alveus (O/A) of CA1 hippocampus and, in addition to CA1, innervate subiculum (Francavilla et al. 2018). Through

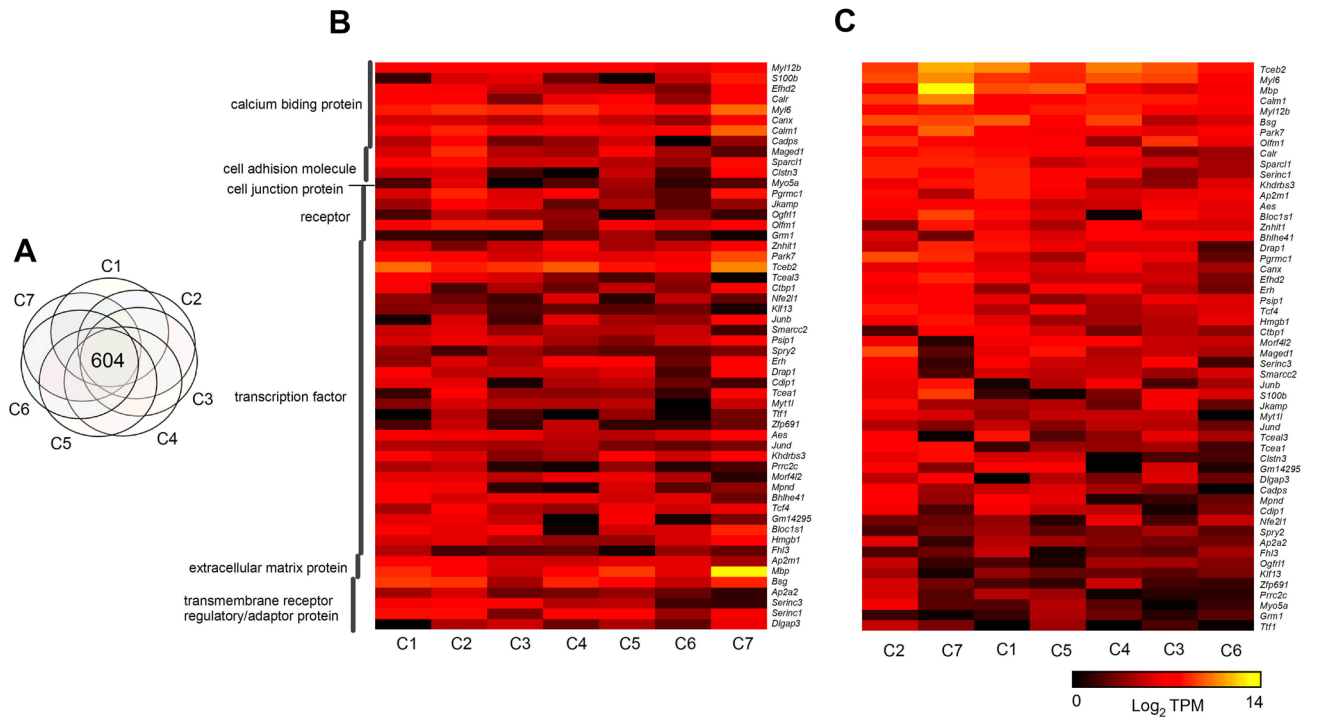

Fig. 3 Heat maps showing the expression values of common genes in all single cell samples. **a** Venn diagram of 604 common genes shared by 7 single cell samples. Each circle indicates the total genes within a single cell sample. The number in the overlaped area indicates the number of common genes (C1–C7 correspond to individual cells). **b** Heat-map for some common genes selected according to protein families. The protein family names were obtained from PANTHER classification system (Mi et al. 2017). The gene names are shown on the right of the heat map. The protein family names are shown on the left side of the heat map. The single cell samples are shown on the bottom (C1–C7). **c** Heat-map indicating the expression levels of common genes. The mean expression values across samples were calculated for each gene and then arranged from top to bottom (high to low). The gene names are indicated on the right. The single cell samples are shown on the bottom (C1–C7). **c** The color scale indicates the logarithm of TPM values to base 2 from low (black) to high (yellow)

preferential synaptic contacts onto interneurons located in the CA1 and conjoint innervation of interneurons and principal cells in subiculum, these cells control the information flow along the hippocampo-subicular axis. Yet, the molecular identity and functional role of the subiculum-projecting VIP+ cells remain unknown. To explore the genetic basis of the input–output transformations and neuromodulatory control in these cells and identify additional discriminant molecular markers that can be used to target them selectively, we obtained their transcriptomic profile using single-cell patch RNA-sequencing (Patch-seq) in combination with electrophysiological recordings and post hoc morphological reconstruction (Cadwell et al. 2016; Fuzik et al. 2016). Following patch-clamp recordings of membrane properties and filling the recorded cells with biocytin, the cell cytoplasm was gently aspirated for transcriptomic analysis (Fig. 1a). From the dataset obtained ($n = 32$ cells), 7 single cell samples satisfied the morphological (Fig. 1b, c, bottom), electrophysiological (Fig. 1b, inset), neurochemical (1c, top) and transcriptomic (Fig. 1d) selection criteria ("Materials and Methods") and were used for gene expression analysis. Selected neurons had a resting membrane potential of -60.0 ± 1.0 mV, an input resistance of 209 ± 41.1 MΩ and a membrane capacitance of 76.5 ± 11.2 pF. They exhibited a regularly spiking firing pattern and a large amplitude Ih current (Ih rectification: 16.1 ± 1.5 mV; Fig. 1b, inset). Post hoc morphological analysis of selected VIP+ cells revealed horizontally oriented dendrites within CA1 O/A with a dominant axonal arborization within the CA1 O/A and projections to proximal subiculum (Fig. 1b, c, bottom), while neurochemical analysis of these cells confirmed that in addition to VIP, they coexpress M2R (Fig. 1c, top) in line with phenotype of the subiculum-projecting VIP+ neurons (Francavilla et al. 2018).

Following the cDNA library construction and next-generation sequencing, the transcriptomic profiles of selected VIP+ cells were analyzed (Fig. 1e). We found that these cells expressed the common VIP+ interneuron genes (*Gad1*, 7 of 7 cells; *Gad2*, 5 of 7 cells; *Vip*, 7 of 7 cells; *Cck,* 4 of 7 cells; and *Chrm2,* 4 of 7 cells) but not the excitatory neuronal (*Emx1, Tbr1,* 0 of 7 cells) or glial (*Gfap,* 0 of 7 cells) transcripts (Fig. 1f), consistent with their GABAergic nature

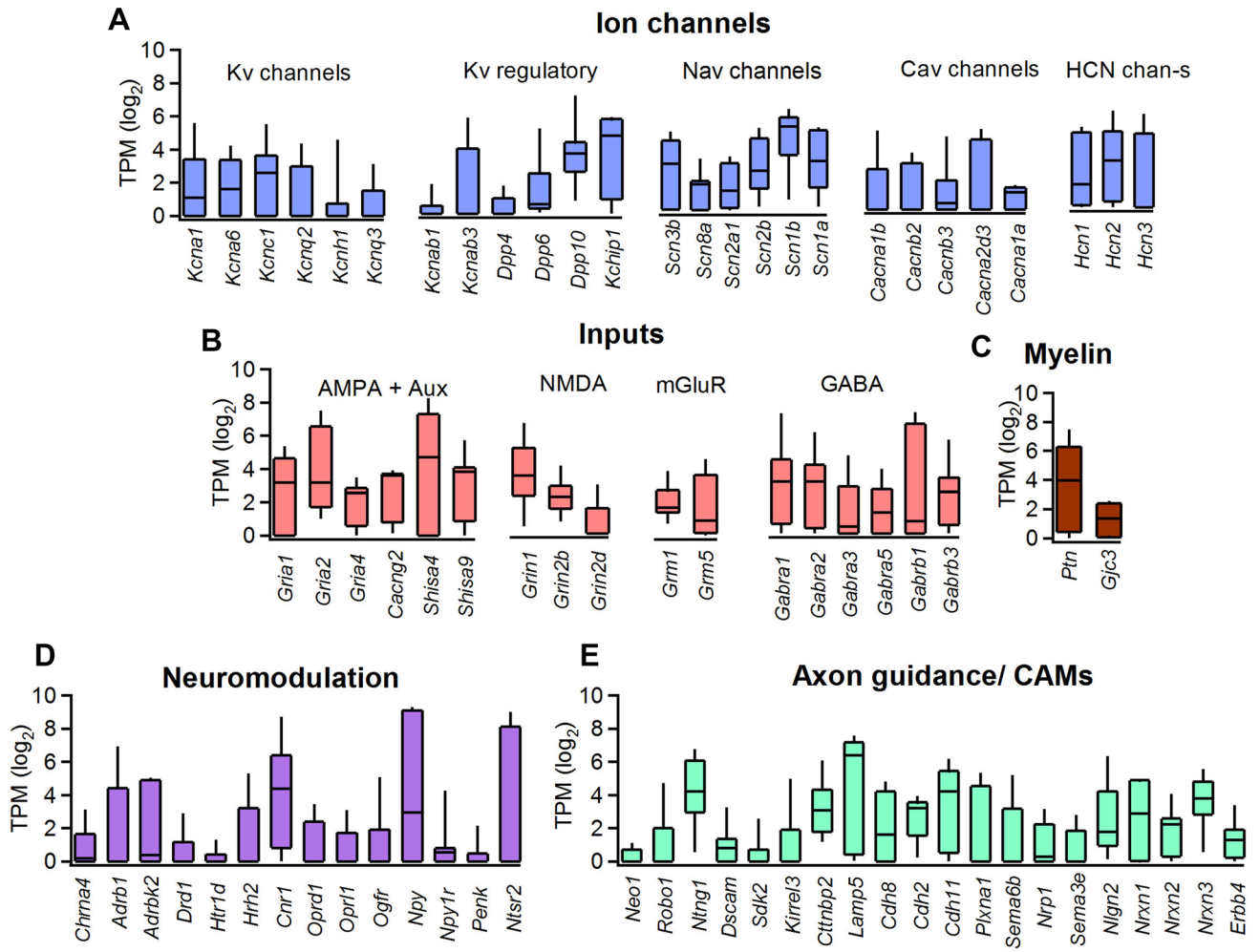

Fig. 4 Boxplots showing selected genes with various expression levels across single cell samples. Summary boxplots showing the expression levels of selected genes for ion channels (**a**, including Kv channels, Kv regulatory elements, Cav channels and HCN chennels), glutamate and GABA receptors (**b** including AMPARs and auxiliary elements, NMDARs, mGluRs and GABARs), myelination factors (**c**), neuromodulatory/neuropeptide signalling, (**d**) and axon guidance/cell adhesion molecules (CAMs, **e**). The upper and lower whiskers show the maximum and minimum values respectively, the lower border and upper border of the box show the 1st and 3rd quartile, the line in the middle of the box indicates the median. The gene expression values are expressed as the logarithm of TPM values to base 2

and VIP+ phenotype. Furthermore, subiculum-projecting VIP+ cells expressed several genes specific for CGE-derived interneurons (Fig. 1g), consistent with their CGE origin. In searching for commonly expressed genes, we examined the transcripts with TPM > 1 across 7 cell samples (Fig. 1e). We extracted the list of common genes between the first two samples, and then explored which genes from this gene list can be found in the next sample. By repeating this process for all samples, we identified 604 common genes that were expressed in all 7 cells (Fig. 3a, Supplementary Table 1). We compared the frequency distribution of all detected genes (total genes) with common genes (Fig. 2a–c). The median expression levels of common genes (median of medians: 6.5 $\log_2$ TPM) were lager than median expression level of total genes (median of medians: 3.8 $\log_2$ TPM, $P < 0.001$ in all cells, one-way ANOVA), indicating the higher expression levels of common genes in all samples.

As the common genes could determine the cell type-specific structure and function, the ontology of common genes was analyzed using the PANTHER Gene List Analysis (Mi et al. 2017). We found that the products of many of these transcripts belonged to important protein families, such as calcium biding proteins (PANTHER protein class: PC00060), cell adhesion molecules (PC00069), cell junction proteins (PC00070), receptors (PC00197), transcription factors (PC00218), extracellular matrix proteins (PC00102), and transmembrane receptor regulatory/adaptor proteins (PC00226, Fig. 3b). Arranging the common

genes within these families by their mean expression values across samples, we identified several highly expressed genes (Fig. 3c). For example, the 10 genes with the highest expression levels included the calcium biding proteins *Myl6* (Myosin Light Chain 6), *Calm1* (Calmodulin 1), *Myl12b* (Myosin Light Chain 12B), and *Calr* (Calreticulin); the cell adhesion molecule *Sparcl1* (SPARC Like 1); the extracellular matrix proteins *Mbp* (Myelin Basic Protein) and *Bsg* (Basigin); the transcription factors *Tceb2* (Transcription Elongation Factor B) and *Park7* (Parkinsonism associated deglycase); and the axonal growth regulator *Olmf1* (Olfactomedin).

We next explored the similarity of the transcriptomic profile of the subiculum-projecting VIP+ cells with other cortical VIP+ interneurons, such as VIP/CR-co-expressing (VIP:CR) interneuron-selective cells and VIP/CCK-co-expressing (VIP:CCK) basket cells (Paul et al. 2017), or hippocampal CA1 interneurons (Harris et al. 2018). We found that many genes that were enriched in cortical VIP:CR interneurons (e.g., *Chrna4, Unc5a*) or in VIP:CCK basket cells (e.g., *Tac2, Cnr1*) (Paul et al. 2017) were detected in the subiculum-projecting VIP+ cells (Supplementary Table 2). Two VIP:CR-specific genes (*Dlgap*3, DLG Associated Protein 3 and *Ptms,* Parathymosin) and one gene detected in long-range projecting somatostatin/nitric oxide synthase-coexpressing (Sst:Nos1) GABAergic neurons (*Nnat,* Neuronatin) were found in all samples, thus corresponding to common genes of the subiculum-projecting VIP+ cells. In addition, the *Pcp4* (Purkinje Cell Protein 4) mRNAs, which were highly enriched in the long-range projecting Sst:Nos1 cells in hippocampal CA1 (Harris et al. 2018), were also detected in all subiculum-projecting VIP+ cell samples, corresponding to the common genes of these cells (Supplementary Table 1). These data indicate that the subiculum-projecting VIP+ cells exhibit transcriptomic profile similar to other VIP+ neurons but share some genes with long-range projecting GABAergic cells.

To predict the intrinsic, synaptic and neuromodulatory properties of the subiculum-projecting VIP+ cells, we next examined the expression of genes within the major functional families, including ion channels, excitatory and inhibitory inputs, neuromodulatory molecules and the axon guidance/cell adhesion molecules (Supplementary Table 2). We compared the frequency distribution of these selected genes within functional gene families with total genes in each cell sample (Fig. 2a, c, d). The distributions followed similar trends in each cell except cell 7. The median expression levels of selected genes (median of medians: 3.4 $\log_2$ TPM) were also similar to those of total genes (median of medians: 3.8 $\log_2$ TPM, $P > 0.05$ in all cells, one-way ANOVA), and the overall expression levels of selected functional genes were variable between samples. We found that these cells exhibit the common ion channel genes within the Kv, Nav and Cav families as well as the cyclic nucleotide-regulated HCN ion channel genes, consistent with a prominent Ih current (Figs. 1b, 4a). In line with previous findings for cortical VIP+ interneurons (Paul et al. 2017), subiculum-projecting VIP+ cells showed roughly similar GluA1 and GluA2 content and expressed GluA4, alone with genes encoding for stargazin and the SHISA family (SHISA4 and SHISA9) AMPA receptor (AMPAR) auxiliary subunits (Fig. 4b). In addition, they expressed genes for NR2B and NR2D NMDA receptor (NMDAR) subunits, and both metabotropic glutamate receptor 1 (mGluR1) (*Grm1*, Fig. 4b) and mGluR5 (*Grm5*, Fig. 4b). Among the constituents of the GABAA receptor (GABAAR), the α1, α2, α3 and α5 as well as β1 and β3 subunits were detected (Fig. 4b). They also expressed the pleiotropin and connexin29 genes (*Ptn* and *Gjc3,* Fig. 4c), both involved in axon myelination (Altevogt et al. 2002; Kuboyama et al. 2015), consistent with a partial myelination of their axon (Francavilla et al. 2018). Furthermore, these cells expressed a large variety of genes involved in neuromodulatory signaling, including acetylcholine (*Chrna4*), norepinephrin (*Adrb1*), dopamine (*Drd1*), serotonin (*Htr1d*), cannabinoid (*Cnr1*), opioid (*Oprd1, Oprl1*), neuropeptide Y (*Npy1r*) and neurotensin (*Ntsr2*) receptors (Fig. 4d), indicating that the subiculum-projecting VIP+ cells are likely modulated via mood, reward and stress-activated neural pathways. In addition to VIP, these cells expressed neuropeptide Y (NPY) and proenkephalin (Penk) (Fig. 4d), suggesting that VIP, NPY and enkephalin peptides can be co-released by these cells under certain conditions. Finally, they expressed the common axon guidance and cell adhesion molecule genes (Fig. 4e), with netrin G1 (*Ntng1*) and cadherin 8 (*Cdh8*) involved in the formation of long-range projections, among others (Lin et al. 2003).

To validate our patch-seq results, we took advantage of a strong M2R expression in the subiculum-projecting VIP+ cells (Francavilla et al. 2018) and performed a triple immunolabeling for VIP-eGFP, M2R and some proteins of interest predicted from the cell transcriptome (Fig. 5a). In addition to Ntng1 identified previously as a long-range axonal marker (Lin et al. 2003), we focused on several proteins detected in hippocampal long-range projecting GABAergic neurons, including the mGluR1a, NPY and Penk (Jinno et al. 2007; Fuentealba et al. 2008). We calculated the percentage of VIP-GFP+ cells located in CA1 O/A that co-express M2R (VIP-GFP+/M2R+) and the marker of interest (mGluR1, NPY, Ntng1 or Penk) and compared these data with VIP-GFP+/M2R– cells. We found that mGluR1a, Ntng1, NPY and Penk were all detected in the M2R+ subiculum-projecting VIP+ cells as predicted from their transcriptomes (Fig. 5a, c). However, these molecules were also expressed in VIP-GFP+/M2R– cells (Fig. 5b, c), indicating that they are not specific for the subiculum-projecting VIP+ neurons. Furthermore, a larger proportion

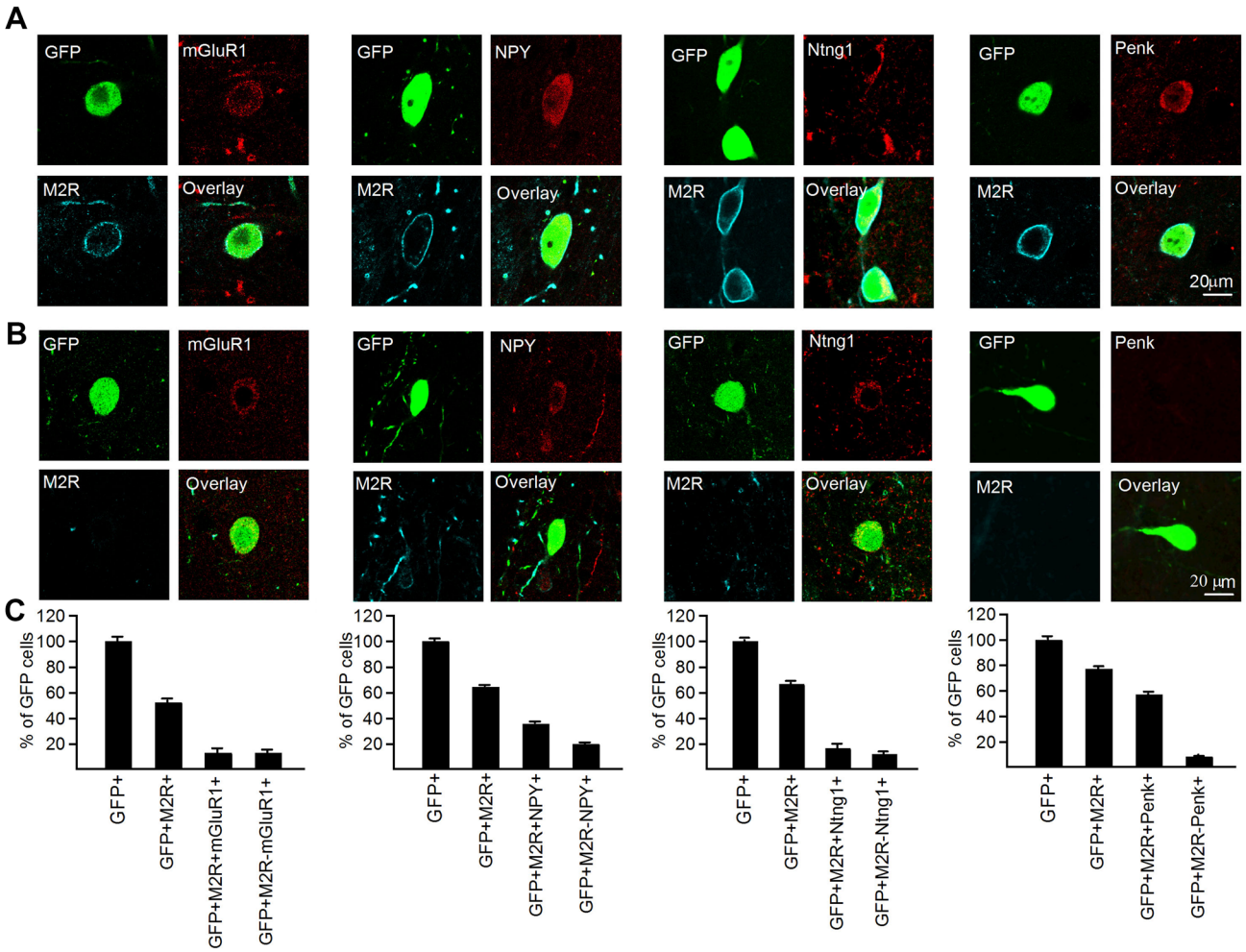

Fig. 5 Additional markers for the subiculum-projecting VIP+ cells obtained following gene expression validation with immunohistochemical analysis. **a** Representative confocal images showing triple immunolabelling in CA1 O/A for VIP-GFP (green), M2R (cyan) and other markers: mGluR1a, NPY, netrin G1, proenkephalin (all in red) as well as the overlay of all. In (**a**), GFP cells co-expressed M2R and other markers. **b** Representative confocal images showing that mGluR1, NPY and Ntng1 were also present in some GFP+ M2R– cells. However, the expression of Penk in GFP + M2R– cells was not frequent. The colors representing different markers are the same as in (**a**, **c**). Bar graphs showing the percentage of GFP cells co-expressing M2R and other markers. mGluR1, NPY and Ntng1 were present in both GFP+ M2R+ and GFP+ M2R– cells, whereas Penk was preferentially co-expressed with GFP and M2R

of VIP-GFP+/M2R+ cells co-expressed Penk, which was detected in only a small number of VIP-GFP+/M2R– cells, indicating that Penk may be more frequently expressed in the subiculum-projecting VIP+ neurons (Fig. 5a–c). Collectively, these data validate results obtained with transcriptomic analysis and identify the subiculum-projecting VIP+ neurons as a member of the VIP+ population, which shares molecular identity and, likely, physiological function with other VIP interneurons, but also has genes associated with specific features (long-range projections and axon myelination) that allow for long-distance coordination.

Discussion

We show that the subiculum-projecting VIP+ neurons in the mouse CA1 hippocampus form a distinct population that can be distinguished based on the M2R and Penk co-expression. Using a transcriptomic analysis based on the patch-sequencing of morphologically identified cells, we found that these cells share molecular identity with both VIP+ interneuron-selective cells and the CCK-coexpressing basket cells (Paul et al. 2017). The additional molecular marker identified here for the subiculum-projecting VIP+ cells, the proenkephalin, is expressed preferentially but not selectively in this VIP+ cell type, which can be useful for preferential targeting

of these cells necessary to provide insights into their physiological organization and behaviour-related functions.

Different types of GABAergic neurons with relatively long distant projections have been described in neocortical and hippocampal networks (Jinno et al. 2007; Miyashita and Rockland 2007; Melzer et al. 2012; Basu et al. 2016). Still, very little is known regarding the physiological properties and network function of these cells due to their low density and absence of specific markers that can be used to target these cells selectively. Our transcriptome analysis can predict some physiological properties and network-state dependent recruitment of these cells. In particular, the subiculum-projecting VIP+ neurons exhibit the GluA1, GluA2 and GluA4 of AMPAR core subunits, as well as the NR1, NR2B and NR2D NMDAR subunits, suggesting that their excitatory synapses contain the Ca^{2+}-impermeable AMPARs and NMDARs. The latter may indicate the generation of the NMDAR-dependent dendritic Ca^{2+}-signals and Hebbian forms of plasticity at excitatory inputs to these cells (Topolnik 2012). They also contain both the mGluR1 and mGluR5, which may be involved in the regulation of the NMDAR-independent Hebbian LTP (Perez et al. 2001; Topolnik 2012). In addition, they express the α1, α2, α3 and α5 as well as β1 and β3-containing GABAARs, pointing to input-specific GABAAR composition, with slow α3 and α5-containing synapses at some inhibitory inputs (Ali and Thomson 2008; Vargas-Caballero et al. 2010; Salesse et al. 2011; Magnin et al. 2019). Thus, the subiculum-projecting VIP+ cells can be sensitive to the α3- and the α5-GABAAR-specific pharmacological manipulations and contribute to the associated cognitive and anxiogenic effects (Navarro et al. 2002; Mohler and Rudolph 2017; Magnin et al. 2019). In addition, these cells express a large variety of neuromodulatory receptors, including acetylcholine, norepinephrine, dopamine and 5-HT receptors, indicating that their recruitment can be controlled by the brain state-dependent modulatory subcortical projections. In terms of output, these cells express NPY and Penk and, therefore, may release these neuropeptides in addition to VIP and GABA. Furthermore, they feature numerous neuropeptide receptors, including cannabinoid, opioid, NPY and neurotensin receptors, highlighting that they are themselves under control of multiple peptidergic influences. In contrast to most GABAergic interneurons, the subiculum-projecting VIP+ cells exhibit a partially myelinated axon and, consistent with this feature, express genes involved in axon myelination, such as *Ptn* and *Gjc3* (Altevogt et al. 2002; Kuboyama et al. 2015). The latter genes together with *Ntng1* and *Cdh8*, which have been involved in long-distance axon guidance, position these cells apart from their VIP+ counterparts. Collectively, this study reveals a molecular profile of a rare subtype of VIP+ projecting neuron that can be recruited through multiple cortical and subcortical inputs to modulate the hippocampo-subicular dialogue.

Finally, emerging evidence has linked the dysfunction of VIP+ interneurons with several neurological and psychiatric disorders. The reduction in NPY and VIP gene expression, as well as the duplication of the VIP receptor *Vipr2* gene copies has been associated with schizophrenia and bipolar disorder in humans (Vacic et al. 2011; Fung et al. 2014). Moreover, Cunniff and Sohal (2017) reported that VIP+ interneurons in the prefrontal cortex of two mouse models of the autism spectrum disorder show abnormal cholinergic responses. In addition, the reduction in NPY+ and VIP+ interneurons has been detected in the hippocampus of human subjects with temporal lobe epilepsy (TLE; De Lanerolle et al. 1989; Sundstrom et al. 2001) and in the pilocarpine-induced experimental chronic TLE (David and Topolnik 2017). Taken together, these findings suggest that impaired circuit coordination by VIP+ interneurons may be associated with several CNS disorders. Among VIP+ cells, the subiculum-projecting CA1 VIP+ cells are well positioned to coordinate the fear memory encoding and retrieval (Roy et al. 2017), the episode recollection (Eldridge et al. 2005), and the initiation and maintenance of epileptic discharges in TLE (Stafstrom 2005). Thus, the transcriptomic profile of the subiculum-projecting VIP+ cells identified in our study may be useful for functional analysis of this cell type, necessary for understanding their functional role under normal and pathological conditions.

Acknowledgements We thank the Next-Generation Sequencing Platform at the Genomics Center, CHU de Québec-Université Laval Research Center for their assistance in the development of single-cell RNA sequencing experiments (Martine Dumont, Stéphane Dubois and Martine Tranchant). Special thanks to Peter Somogyi, Olivier Camiré and Kenneth Harris for stimulating discussions and critical comments on the previous version of the manuscript; Sarah Côté and Stéphanie Racine-Dorval for technical assistance and Anton Topolnik for help with data analysis. This work was supported by the Canadian Institutes of Health Research (CIHR Grant #MOP-137072, MOP-142447) and the Natural Sciences and Engineering Research Council of Canada (NSERC Grant #342292-2012) to L.T.

Author contribution statement XL and EMP performed experiments; XL, RF, MV and AD analysed the data; XL and LT wrote the manuscript; LT supervised the whole study.

Data availability statement The RNA-sequencing data obtained in this study have been deposited to public library: GEO (accession # GSE109755).

Compliance with ethical standards

Competing interest The authors have no competing interests to report.

Ethical approval and informed consent: All experiments on mice were approved by the Animal Protection Committee of Université Laval and

the Canadian Council on Animal Care, and carried out in accordance with relevant guidelines and regulations.

References

Acsády L, Gorcs TJ, Freund TF (1996a) Different populations of vasoactive intestinal polypeptide-immunoreactive interneurons are specialized to control pyramidal cells or interneurons in the hippocampus. Neuroscience 73:317–334

Acsády L, Arabadzisz D, Freund T (1996b) Correlated morphological and neurochemical features identify different subsets of vasoactive intestinal polypeptide-immunoreactive interneurons in rat hippocampus. Neuroscience 73:299–315

Ali AB, Thomson AM (2008) Synaptic alpha 5 subunit-containing GABAA receptors mediate IPSPs elicited by dendrite-preferring cells in rat neocortex. Cereb Cortex 18:1260–1271. https://doi.org/10.1093/cercor/bhm160

Altevogt BM, Kleopa KA, Postma FR, Scherer SS, Paul DL (2002) Connexin29 is uniquely distributed within myelinating glial cells of the central and peripheral nervous systems. J Neurosci 22:6458–6470

Ayzenshtat I, Karnani MM, Jackson J, Yuste R (2016) Cortical control of spatial resolution by VIP + interneurons. J Neurosci 36:11498–11509. https://doi.org/10.1523/jneurosci.1920-16.2016

Basu J, Zaremba JD, Cheung SK, Hitti FL, Zemelman BV, Losonczy A, Siegelbaum SA (2016) Gating of hippocampal activity, plasticity, and memory by entorhinal cortex long-range inhibition. Science 351:aaa5694. https://doi.org/10.1126/science.aaa5694

Bayraktar T, Welker E, Freund TF, Zilles K, Staiger JF (2000) Neurons immunoreactive for vasoactive intestinal polypeptide in the rat primary somatosensory cortex: morphology and spatial relationship to barrel-related columns. J Comp Neurol 420:291–304

Brennecke P et al (2013) Accounting for technical noise in single-cell RNA-seq experiments. Nat Methods 10:1093–1095. https://doi.org/10.1038/nmeth.2645

Cadwell CR et al (2016) Electrophysiological, transcriptomic and morphologic profiling of single neurons using. Patch-seq Nat Biotechnol 34:199–203. https://doi.org/10.1038/nbt.3445

Chamberland S, Salesse C, Topolnik D, Topolnik L (2010) Synapse-specific inhibitory control of hippocampal feedback inhibitory circuit. Front Cell Neurosci 4:130. https://doi.org/10.3389/fncel.2010.00130

Cunniff M, Sohal V (2017) VIP interneuron cholinergic responses are altered in multiple models of autism. Biol Psychiatry 81:138. https://doi.org/10.1016/j.biopsych.2017.02.351

David LS, Topolnik L (2017) Target-specific alterations in the VIP inhibitory drive to hippocampal GABAergic cells after status epilepticus. Exp Neurol 292:102–112. https://doi.org/10.1016/j.expneurol.2017.03.007

de Lanerolle NC, Kim JH, Robbins RJ, Spencer DD (1989) Hippocampal interneuron loss and plasticity in human temporal lobe epilepsy. Brain Res 495:387–395

Eldridge LL, Engel SA, Zeineh MM, Bookheimer SY, Knowlton BJ (2005) A dissociation of encoding and retrieval processes in the human hippocampus. J Neurosci 25:3280–3286. https://doi.org/10.1523/JNEUROSCI.3420-04.2005

Foldy C, Darmanis S, Aoto J, Malenka RC, Quake SR, Sudhof TC (2016) Single-cell RNAseq reveals cell adhesion molecule profiles in electrophysiologically defined neurons. Proc Natl Acad Sci USA 113:E5222–5231. https://doi.org/10.1073/pnas.1610155113

Francavilla R, Villette V, Luo X, Chamberland S, Munoz-Pino E, Camire O, Wagner K, Kis V, Somogyi P, Topolnik L (2018) Connectivity and network state-dependent recruitment of long-range VIP-GABAergic neurons in the mouse hippocampus. bioRxiv. https://doi.org/10.1101/364547

Fu Y, Tucciarone JM, Espinosa JS, Sheng N, Darcy DP, Nicoll RA, Huang ZJ, Stryker MP (2014) A cortical circuit for gain control by behavioral state. Cell 156:1139–1152. https://doi.org/10.1016/j.cell.2014.01.050

Fuentealba P, Tomioka R, Dalezios Y, Marton LF, Studer M, Rockland K, Klausberger T, Somogyi P (2008) Rhythmically active enkephalin-expressing GABAergic cells in the CA1 area of the hippocampus project to the subiculum and preferentially innervate interneurons. J Neurosci 28:10017–10022. https://doi.org/10.1523/JNEUROSCI.2052-08.2008

Fung SJ, Fillman SG, Webster MJ, Shannon Weickert C (2014) Schizophrenia and bipolar disorder show both common and distinct changes in cortical interneuron markers. Schizophr Res 155:26–30. https://doi.org/10.1016/j.schres.2014.02.021

Fuzik J, Zeisel A, Máté Z, Calvigioni D, Yanagawa Y, Szabó G, Linnarsson S, Harkany T (2016) Integration of electrophysiological recordings with single-cell RNA-seq data identifies neuronal subtypes. Nat Biotechnol 34:175–183

Gonchar Y, Wang Q, Burkhalter A (2007) Multiple distinct subtypes of GABAergic neurons in mouse visual cortex identified by triple immunostaining. Front Neuroanat 1:3. https://doi.org/10.3389/neuro.05.003.2007

Grun D, van Oudenaarden A (2015) Design and analysis of single-cell sequencing experiments. Cell 163:799–810. https://doi.org/10.1016/j.cell.2015.10.039

Harris KD, Hochgerner H, Skene NG, Magno L, Katona L, Bengtsson Gonzales C, Somogyi P, Kessaris N, Linnarsson S, Hjerling-Leffler J (2018) Classes and continua of hippocampal CA1 inhibitory neurons revealed by single-cell transcriptomics. PLoS Biol 16:e2006387. https://doi.org/10.1371/journal.pbio.2006387

He M, Tucciarone J, Lee S, Nigro MJ, Kim Y, Levine JM, Kelly SM, Krugikov I, Wu P, Chen Y, Gong L, Hou Y, Osten P, Rudy B, Huang ZJ (2016) Strategies and Tools for Combinatorial Targeting of GABAergic Neurons in Mouse Cerebral Cortex. Neuron 92:555. https://doi.org/10.1016/j.neuron.2016.10.009

Jinno S et al (2007) Neuronal diversity in GABAergic long-range projections from the hippocampus. J Neurosci 27:8790–8804. https://doi.org/10.1523/JNEUROSCI.1847-07.2007

Klausberger T, Somogyi P (2008) Neuronal diversity and temporal dynamics: the unity of hippocampal circuit operations. Science 321:53–57. https://doi.org/10.1126/science.1149381321/5885/53

Kuboyama K, Fujikawa A, Suzuki R, Noda M (2015) Inactivation of protein tyrosine phosphatase receptor type Z by pleiotrophin promotes remyelination through activation of differentiation of oligodendrocyte precursor cells. J Neurosci 35:12162–12171. https://doi.org/10.1523/JNEUROSCI.2127-15.2015

Lee S, Kruglikov I, Huang ZJ, Fishell G, Rudy B (2013) A disinhibitory circuit mediates motor integration in the somatosensory cortex. Nat Neurosci 16:1662–1670. https://doi.org/10.1038/nn.3544

Lin JC, Ho WH, Gurney A, Rosenthal A (2003) The netrin-G1 ligand NGL-1 promotes the outgrowth of thalamocortical axons. Nat Neurosci 6:1270–1276. https://doi.org/10.1038/nn1148

Madisen L et al (2015) Transgenic mice for intersectional targeting of neural sensors and effectors with high specificity and performance. Neuron 85:942–958. https://doi.org/10.1016/j.neuron.2015.02.022

Magnin E, Francavilla R, Amalyan S, Gervais E, David L, Luo X, Topolnik L (2019) Input specific synaptic location and function of the alpha5 GABAA receptor subunit in the mouse CA1 hippocampal neurons. J Neurosci 39:788–801. https://doi.org/10.1523/jneurosci.0567-18.2018

Melzer S, Michael M, Caputi A, Eliava M, Fuchs EC, Whittington MA, Monyer H (2012) Long-range-projecting GABAergic neurons modulate inhibition in hippocampus and entorhinal cortex. Science 335:1506–1510. https://doi.org/10.1126/science.1217139

Mi H, Huang X, Muruganujan A, Tang H, Mills C, Kang D, Thomas PD (2017) PANTHER version 11: expanded annotation data from Gene Ontology and Reactome pathways, and data analysis tool enhancements. Nucleic Acids Res 45:D183–D189. https://doi.org/10.1093/nar/gkw1138

Miyashita T, Rockland KS (2007) GABAergic projections from the hippocampus to the retrosplenial cortex in the rat. Eur J Neurosci 26:1193–1204. https://doi.org/10.1111/j.1460-9568.2007.05745.x

Miyoshi G et al (2015) Prox1 Regulates the subtype-specific development of caudal ganglionic eminence-derived GABAergic cortical interneurons. J Neurosci 35:12869–12889. https://doi.org/10.1523/jneurosci.1164-15.2015

Mohler H, Rudolph U (2017) Disinhibition, an emerging pharmacology of learning and memory. F1000Res. https://doi.org/10.12688/f1000research.9947.1

Navarro JF, Buron E, Martin-Lopez M (2002) Anxiogenic-like activity of L-655,708, a selective ligand for the benzodiazepine site of GABA(A) receptors which contain the alpha-5 subunit, in the elevated plus-maze test. Prog Neuropsychopharmacol Biol Psychiatry 26:1389–1392

Paul A, Crow M, Raudales R, He M, Gillis J, Huang ZJ (2017) Transcriptional architecture of synaptic communication delineates GABAergic neuron identity. Cell 171(522–539):e520. https://doi.org/10.1016/j.cell.2017.08.032

Perez Y, Morin F, Lacaille JC (2001) A hebbian form of long-term potentiation dependent on mGluR1a in hippocampal inhibitory interneurons. Proc Natl Acad Sci USA 98:9401–9406. https://doi.org/10.1073/pnas.161493498

Petilla Interneuron Nomenclature G et al (2008) Petilla terminology: nomenclature of features of GABAergic interneurons of the cerebral cortex. Nat Rev Neurosci 9:557–568. https://doi.org/10.1038/nrn2402

Pi HJ, Hangya B, Kvitsiani D, Sanders JI, Huang ZJ, Kepecs A (2013) Cortical interneurons that specialize in disinhibitory control. Nature 503:521–524. https://doi.org/10.1038/nature12676

Porter JT, Cauli B, Staiger JF, Lambolez B, Rossier J, Audinat E (1998) Properties of bipolar VIPergic interneurons and their excitation by pyramidal neurons in the rat neocortex. Eur J Neurosci 10:3617–3628

Risso D, Ngai J, Speed TP, Dudoit S (2014) Normalization of RNA-seq data using factor analysis of control genes or samples. Nat Biotechnol 32:896–902. https://doi.org/10.1038/nbt.2931

Roy DS, Kitamura T, Okuyama T, Ogawa SK, Sun C, Obata Y, Yoshiki A, Tonegawa S (2017) Distinct Neural Circuits for the Formation and Retrieval of Episodic Memories. Cell 170(1000–1012):e1019. https://doi.org/10.1016/j.cell.2017.07.013

Salesse C, Mueller CL, Chamberland S, Topolnik L (2011) Age-dependent remodelling of inhibitory synapses onto hippocampal CA1 oriens-lacunosum moleculare interneurons. J Physiol 589:4885–4901. https://doi.org/10.1113/jphysiol.2011.215244

Somogyi P (2010) Hippocampus: Intrinsic Organisation. In: Shepherd G, Grillner S (eds) Handbook of brain microcircuits. Oxford University Press, Oxford, pp 148–664

Somogyi J, Baude A, Omori Y, Shimizu H, El Mestikawy S, Fukaya M, Shigemoto R, Watanabe M, Somogyi P (2004) GABAergic basket cells expressing cholecystokinin contain vesicular glutamate transporter type 3 (VGLUT3) in their synaptic terminals in hippocampus and isocortex of the rat. Eur J Neurosci 19:552–569. https://doi.org/10.1111/j.0953-816X.2003.03091.x

Stafstrom CE (2005) The role of the subiculum in epilepsy and epileptogenesis. Epilepsy Curr 5:121–129. https://doi.org/10.1111/j.1535-7511.2005.00049.x

Sundstrom LE, Brana C, Gatherer M, Mepham J, Rougier A (2001) Somatostatin- and neuropeptide Y-synthesizing neurones in the fascia dentata of humans with temporal lobe epilepsy. Brain 124:688–697

Taniguchi H, He M, Wu P, Kim S, Paik R, Sugino K, Kvitsiani D, Fu Y, Lu J, Lin Y, Miyoshi G, Shima Y, Fishell G, Nelson SB, Huang ZJ (2011) A resource of Cre driver lines for genetic targeting of GABAergic neurons in cerebral cortex. Neuron 71:101–995. https://doi.org/10.1016/j.neuron.2011.07.026

Tasic B et al (2016) Adult mouse cortical cell taxonomy revealed by single cell transcriptomics. Nat Neurosci 19:335–346. https://doi.org/10.1038/nn.4216

Topolnik L (2012) Dendritic calcium mechanisms and long-term potentiation in cortical inhibitory interneurons. Eur J Neurosci 35:496–506. https://doi.org/10.1111/j.1460-9568.2011.07988.x

Tyan L et al (2014) Dendritic inhibition provided by interneuron-specific cells controls the firing rate and timing of the hippocampal feedback inhibitory circuitry. J Neurosci 34:4534–4547. https://doi.org/10.1523/JNEUROSCI.3813-13.2014

Vacic V et al (2011) Duplications of the neuropeptide receptor gene VIPR2 confer significant risk for schizophrenia. Nature 471:499–503. https://doi.org/10.1038/nature09884

Vargas-Caballero M, Martin LJ, Salter MW, Orser BA, Paulsen O (2010) alpha5 Subunit-containing GABA(A) receptors mediate a slowly decaying inhibitory synaptic current in CA1 pyramidal neurons following Schaffer collateral activation. Neuropharmacology 58:668–675. https://doi.org/10.1016/j.neuropharm.2009.11.005

Zeisel A et al (2015) Brain structure. Cell types in the mouse cortex and hippocampus revealed by single-cell RNA-seq Science 347:1138–1142. https://doi.org/10.1126/science.aaa1934